

# Long-time variations of precipitable water vapour estimated from GPS, MODIS and radiosonde observations in Turkey

Gokhan Gurbuz<sup>a</sup> and Shuanggen Jin<sup>a,b,\*</sup>

<sup>a</sup> Department of Geomatics Engineering, Faculty of Engineering, Bulent Ecevit University, Zonguldak, Turkey

<sup>b</sup> Shanghai Astronomical Observatory, Chinese Academy of Sciences, Shanghai, China

**ABSTRACT:** Water vapour and its variations in the Earth's atmosphere are related to atmospheric activities and climate changes. However, it is difficult to obtain high-resolution and high-accuracy precipitable water vapour (PWV) and its variations using traditional techniques, particularly in Turkey with the complex weather variability caused by the proximity of the Black Sea and the Mediterranean Sea. Satellite observations provide unique ways to observe PWV variations at regional or global scale, e.g. global positioning system (GPS). In this study, long-time PWV variations and trends are investigated and obtained from 6-year continuous GPS observations in Turkey (January 2010–January 2016), which are compared with nearly co-located radiosonde and moderate resolution imaging spectroradiometer (MODIS) observations to check its accuracy. The root mean square error (RMSE) of PWV differences is about 1–3 mm between radiosonde and GPS, and 3–7 mm between MODIS and GPS. Furthermore, the linear trend and seasonal amplitudes, and phase of the GPS-estimated PWV signals are computed. Statistically significant trends are found at all stations. While stations near the Mediterranean Sea have increasing trends with about 0.30 mm year<sup>-1</sup>, the stations at inland have increasing trends of about 0.10 mm year<sup>-1</sup>. The annual phases between radiosonde, GPS and MODIS PWV at all the stations are almost close to each other with differences in 1°–2°. Finally, the relation between north Atlantic oscillation (NAO) and PWV trends is investigated. Results show that PWV trends agree with NAO behaviours especially for the stations near the Mediterranean Sea. The recent human activities may have impacts on long-term PWV variation trends.

**KEY WORDS** precipitable water vapour; MODIS; GPS; radiosonde; climate change

Received 26 October 2016; Revised 27 April 2017; Accepted 28 April 2017

## 1. Introduction

The water vapour is one of the major greenhouse gases in the atmosphere, and its spatiotemporal variations are one of the key issues about climate change at regional and global scales (Mockler, 1995; Held and Soden, 2000; Trenberth *et al.*, 2005; Wagner *et al.*, 2006). It is also a key component in the global energy cycle through surface evaporation and atmospheric latent heating (Trenberth *et al.*, 2009). Precipitable water vapour (PWV) can be defined as the total atmospheric water vapour contained in a vertical column from the ground to the specified height in the troposphere (Ferrare *et al.*, 2002). It is important to observe highly accurate water vapour for accurate weather forecast and atmospheric study. Observing and understanding long-time variations of PWV and its relation with climate are primary objectives. While traditional techniques are difficult to obtain high-resolution and high-accuracy PWV and its variations, particularly in Turkey with the complex weather variability around the Black Sea and the Mediterranean Sea. Since atmospheric delay is one of the main errors in satellite techniques, it

can be estimated in contrast and widely used nowadays (Chaboureaud *et al.*, 1998; Jin *et al.*, 2004, 2006, 2007a, 2014a, 2015, 2016, 2017; Afraimovich *et al.*, 2010; Wu *et al.*, 2010). Firstly, the global positioning system (GPS) plays a significant role in determining continuous and precise Zenith tropospheric delay (ZTD) and PWV with the high temporal resolution (Jin and Luo, 2009; Jin *et al.*, 2011a, 2011b) and high accuracy (1–2 mm) (Ware *et al.*, 2000). Secondly, the moderate resolution imaging spectroradiometer (MODIS) is an orbiting satellite platform with a number of instruments (Salomonson *et al.*, 1989; King *et al.*, 1992; Asrar and Greenstone, 1995) and also provides PWV data at large scale (Asrar and Greenstone, 1995). Thirdly, the radiosonde technique is the most important as the *in situ* observation technique to estimate PWV (Wang *et al.*, 2007). The radiosonde systems as ground *in situ* measurements often contain systematic errors and low temporal resolution of twice per day, subject to weather conditions (Wang *et al.*, 2002).

In this study, the long-time PWV time series are obtained from 6-year continuous GPS observations in Turkey (2010–2016). Results are compared with nearly co-located radiosonde observations and MODIS observations for the first time in Turkey. Apart from evaluating the estimated PWV values with their RMSE's and correlations, analyses are carried out to understand the trends

\* Correspondence to: S. Jin, Shanghai Astronomical Observatory, Chinese Academy of Sciences, 80 Nandan Road, Shanghai 200030, China. E-mail: sgjin@shao.ac.cn; or sgjin@beun.edu.tr

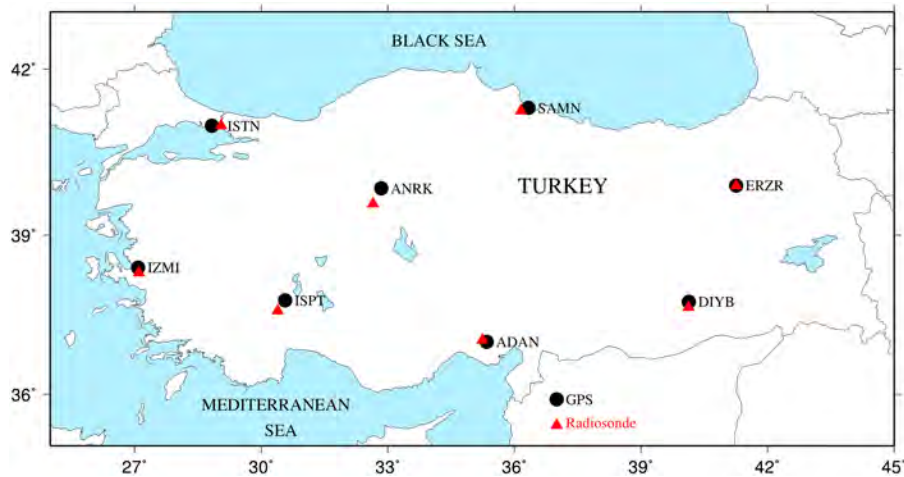


Figure 1. Distribution of co-located GPS and radiosonde stations in Turkey. [Colour figure can be viewed at [wileyonlinelibrary.com](http://wileyonlinelibrary.com)].

and annual and semi-annual variations of PWV time series from three techniques. The long-term trends are confirmed using the nonparametric Mann–Kendall test to statistically assess if there is an increasing or decreasing trend of the variable of interest over the studied time (Mann, 1945; Kendall, 1975; Gilbert, 1987). Especially long-term trend behaviours are investigated by analyzing the relation between PWV trends and oscillation indexes such as El-Nino southern oscillation (ENSO) and north Atlantic oscillation (NAO) in the Mediterranean climate.

## 2. Data and methods

### 2.1. Radiosonde observations

The routine radiosonde observations have undoubtedly been a significant contribution to our understanding of the global atmosphere circulation, hydrological cycle and local dynamical processes. The global radiosonde network provides a considerable resource of humidity observations through much of the twentieth century. The radiosonde is a combination of sensors that can measure the pressure, temperature and humidity while ascending with the help of weather balloon, and transmit gathered information via radio signals to the ground station.

Turkey has eight radiosonde stations throughout its territory, which are distributed evenly as possible (Figure 1). These radiosonde stations, launch radiosonde balloons twice in a day (0000, 1200 UTC) are under the administration of Turkish Met-Office (Meteoroloji Genel Müdürlüğü). Pre-processed radiosonde data from 1 January 2010 to 31 December 2015 are obtained from the University of Wyoming's website (<http://weather.uwyo.edu/upperair>). The PWV can be estimated from the temperature  $T$  ( $^{\circ}\text{C}$ ), atmospheric pressure  $P$  (hPa), and relative humidity  $RH$  (%) measured by radiosondes as:

$$\text{PWV} = \frac{10^3}{\rho} \int_{z=0}^{z=1} \rho_w dz \quad (1)$$

where  $\rho$  and  $\rho_w$  are the liquid water and water vapour density, respectively ( $\text{kg m}^{-3}$ ) obtained from radiosonde, the ground is  $z_0$  and highest altitude is  $z_1$  (m).

### 2.2. GPS observations

The daily GPS data used in this study are obtained from the Bundesamt für Kartographie und Geodäsie (BKG) ([igs.bkg.bund.de](http://igs.bkg.bund.de)) and TUSAGA-Active ([rinex.tusaga-aktif.gov.tr](http://rinex.tusaga-aktif.gov.tr)). GAMIT/Globk software is used to estimate daily coordinates and Zenith tropospheric delay (ZTD) parameters (Jin *et al.*, 2007b, 2009). Meteorological observations which are used in the PWV estimations are obtained from Turkish Met-Office, and RINEX.m files are created using these parameters. Final products of International GNSS Service (IGS) as precise orbit, tidal and non-tidal atmospheric pressure loading (ATML) with the Earth's centre of mass frame (CM) (Tregoning and van Dam, 2005) are used in the GAMIT software (Jin and Park, 2006; Herring *et al.*, 2015). The second- and third-order ionospheric effects were neglected in the processing. As for tropospheric parameters, two different strategies with Vienna mapping function (VMF1) and Niell mapping function (NMF) are used to estimate PWV in GAMIT. Zenith hydrostatic delay (ZHD) values are calculated using the atmospheric pressure and the height (km) above the geoid as:

$$\text{ZHD} = \frac{2.2768 + 0.0005}{1 - 0.00266 \cos(2\phi) - 0.00028 h} p \quad (2)$$

where  $\phi$  is the latitude,  $h$  is the height from the geoid and  $p$  is the atmospheric pressure at the antenna height. Then Zenith wet delay (ZWD) is obtained by extracting ZHD from ZTD (Jin *et al.*, 2008, 2014b). Using ZWD, the hourly PWV values are computed with `Sh_Met_Util`. Bevis *et al.* (1992) first proposed the concept of GPS meteorology and introduced the principle of GPS to estimate water vapour in detail. Moreover, they proposed the method to calculate  $T_m$ , the critical parameter to transfer ZWD into PWV, which made GPS an essential means to estimate water vapour. The relation between

PWV and ZWD is expressed as (Bevis *et al.*, 1994; Jin and Luo, 2009):

$$\text{PWV} = \Pi \times \text{ZWD} \quad (3)$$

where  $\Pi$  is a water vapour conversion factor, which can be expressed as:

$$\Pi = \frac{10^6}{\rho R_v [(k_3/T_m + k'_2)]} \quad (4)$$

where  $\rho$  is the density of liquid water,  $R_v$  is the specific gas constant for water vapour,  $k_3$  and  $k'_2$  are physical constants, and  $T_m$  is the mean temperature of the atmosphere, which can be computed from surface temperature as  $T_m = 70.2 + 0.72T_s$  (Bevis *et al.*, 1994). In order to estimate most accurate PWV using GPS observations, several processing strategies are evaluated, including using local  $T_m$  model from *in situ* observations, different mapping functions, and various ocean tide loading (OTL) models.

### 2.3. MODIS observations

Level 2 PWV products of MODIS are generated at  $1 \times 1 \text{ km}^2$  spatial resolution using near infrared (NIR) and  $1 \times 5 \text{ km}^2$  using infrared (IR) (Gao and Kaufman, 2003). The method to retrieve water vapour is based on a differential absorption technique which largely removes the surface reflectance with wavelength effects and can retrieve PWV with errors lower than 10% (Kaufman and Gao, 1992; King *et al.*, 2003). Data from 1 January 2010 to 31 December 2015 for longitude  $25^\circ$ – $45^\circ\text{E}$  and latitude  $35^\circ$ – $45^\circ\text{N}$  (Figure 1) are used from National Aeronautics and Space Administration (NASA), Atmosphere Archive and Distribution System (LAADS) (ladsweb.nascom.nasa.gov). Since the IR and NIR observations are sensitive to clouds in the vicinity (Chang *et al.*, 2014), the cloud-free conditioned MODIS-PWV data (MOD05) collected from the Terra platform are used in this study with the help of MODIS cloud mask product. In order to compare results with radiosonde and GPS observations, MODIS-PWVs are averaged using surrounding pixels. For temporal equality, MODIS data are interpolated linearly with 3 h time interval.

In order to evaluate the performance of MODIS-PWV and GPS-PWV, correlation analysis is carried out using radiosonde PWV as a reference. MODIS-PWV values are analyzed using the average value of the closest pixel to the GPS site and its surrounding pixels. After checking all the data, especially the data in winter periods with MODIS cloud mask product for being cloud-free at designated coordinates, only 61% of all observations are used in this study. The mean biases between each technique (MODIS–GPS, MODIS–Radiosonde and GPS–Radiosonde), root mean square errors (RMSEs) and correlation coefficients are computed.

### 2.4. Method to analyze PWV variations

The long-term and seasonal variations of PWV are analyzed using the following harmonic function

with including phase, amplitude and trend (Jin and Feng, 2013) as:

$$\text{PWV}_t = a + bt + \sum_{i=1}^2 [S_i \sin(2\pi(t - t_0)/p_i + \phi_i)] + \varepsilon_t \quad (5)$$

where  $t$  is the time (days),  $t_0$  is 1 January 2010,  $a$  is the constant term,  $b$  is the trend term,  $S_i$ ,  $p_i$  and  $\phi_i$  are the amplitude, period and phase at periods ( $i=1$  and 0.5 year), respectively, and  $\varepsilon_t$  is the residual. Using the least squares method, the annual and semi-annual amplitudes, phases and trend of the GPS-estimated PWV are determined as well as their uncertainties. Also, to investigate trends statistically the Mann–Kendall trend test is applied, which is mostly used in meteorological time series to detect climatic changes. Mann–Kendall trend test is a nonparametric (distribution-free) method that does not take into account the numerical values of the observations, but their ranks are relative to each other and outliers do not distort the results. Moreover, the normality of the residuals is not a necessary condition. In addition to initial Mann–Kendall trend test, the seasonal Mann–Kendall trend test is used for the nonparametric trend analysis of seasonal data (Hirsch *et al.*, 1982). It is a modified form of the original Mann–Kendall trend test with taking into account the seasonality of environmental time series. It is a hypothesis test in which the null hypothesis states that the data are independently and identically distributed. The alternative hypothesis states that the data are not identically distributed (Albek, 2002).

## 3. Evaluation and analysis

In order to assess the accuracy of Bevis  $T_m$  model, a secondary processing method was carried out using the  $T_m$  model, which is developed from Turkish radiosonde observations. The Bevis  $T_m$  and Turkey  $T_m$  models agree well with the radiosonde with high correlation coefficient ( $R^2$ ) and low RMSE values. Also to compare and check the accuracy of GPS-estimated PWV, VMF1 (Boehm *et al.*, 2006) is used and compared with NMF (Niell, 1996). In the strategies with different mapping functions, no apparent or significant differences are found. As stated in Tuka and El-Mowafy (2013), both mapping functions performed well especially above an elevation angle of  $15^\circ$ . In the study of Gurbuz and Jin (2016), five different GPS solutions were carried out to assess the effect of the ocean tide models on the PWV using different OTL models (e.g. Eanes, 1994; Ray, 1999; Matsumoto *et al.*, 2000; Lyard *et al.*, 2006). The ocean tide model FES2004 provided the most accurate results when compared to radiosonde at four GPS stations with RMSE of 2.12 mm in PWV at stations near the coastline. Results showed that the most accurate strategy is using Bevis  $T_m$ , VMF1 and FES2004 models, and therefore these parameters are used for the analysis and evaluations with other techniques.

Inter-comparisons are made to see the performance of GPS-estimated PWV, Radiosonde PWV and MODIS

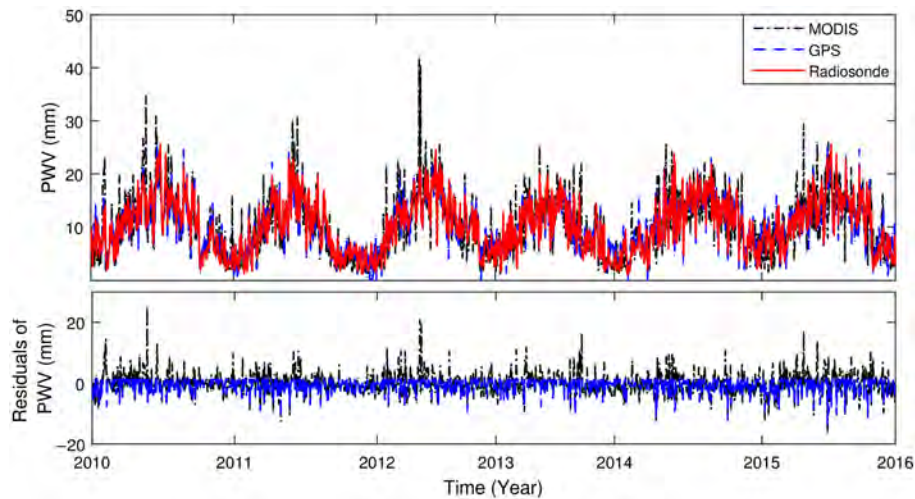


Figure 2. PWV and PWV residuals time series from MODIS, GPS and Radiosonde at ADAN station. [Colour figure can be viewed at [wileyonlinelibrary.com](http://wileyonlinelibrary.com)].

NIR PWV (Figure 2). RMSE of GPS-estimated PWV are 1–3 mm at all stations when compared to Radiosonde PWV. Especially GPS-estimated PWV values at ERZR station performed the best with RMSE of 1.67 and 0.04 mm mean differences with Radiosonde PWV (Table 1). The correlation coefficients of six stations are 0.91 or higher while their biases are lower than 1 mm except ADAN station that is close to the coastline of the Mediterranean Sea and SAMN station that is close to the coastline of the Black Sea (Figure 3). Similar to Gurbuz and Jin (2016), the inland stations have lower GPS-PWV RMSEs, meaning that they have a better agreement with Radiosonde PWV. This could be due to less effect from the ocean tide loading on inland stations like ERZR and ANKR (Table 1).

Correlation coefficients for MODIS NIR PWV and GPS-estimated PWV varies from 0.72 up to 0.81 (Figure 3). Such high correlations and low RMSE values show that MODIS NIR PWV has high accuracy but not as high as GPS-estimated PWV (Figure 3). Therefore, with such accuracy and  $1 \times 1 \text{ km}^2$  resolution, MODIS NIR PWV can be used even for meteorology and climatology studies. The MODIS NIR PWV obtained from Terra platform has lower RMSE's than 6 mm (Figure 3), which agrees with the study of Liu *et al.*, 2015. Both NIR and IR observations tend to overestimate with the increase of PWV values. Inland stations have lower RMSE values than the other stations (Table 2), such as ERZR (RMSE of 3.46 mm with 0.08 mm bias) and ISPT (RMSE of 3.90 mm with 1.41 mm bias). However, all stations have high correlation coefficients from 0.74 up to 0.81 with Radiosonde PWV observations (Table 3).

Previous studies showed that there were some differences between day and night MODIS IR PWV retrieval accuracy (Seemann *et al.*, 2003; 2008; Liu *et al.*, 2015) so PWV values from night and day observations are separated from each other and compared (Figure 4). The RMSE differences between MODIS IR PWV and Radiosonde at day time (4–5 mm) and night time (3–4 mm) data are

nearly 1 mm for each station except for the inland stations like ISPT (0.3 mm), DIYB (0.4 mm), and ERZR (0.3 mm), which have small PWV values with 0.8 mm biases. It is a slight overestimation for large PWV values, whose locations are near the coastline at day time. As noted in Figure 4, during night time MODIS IR PWV has a better agreement than day time with the Radiosonde PWV.

#### 4. PWV variations and discussions

##### 4.1. Seasonal PWV variations

The PWV values have a strong seasonal signal which agrees well for nearly all strategies used in this study. Figure 5 shows annual and semi-annual amplitudes, and phases of the PWV for the used stations in Turkey from GPS, MODIS and Radiosonde during the period of 2010–2016 (Table 2). It has been found that the MODIS has a good agreement with both GPS and Radiosonde in the annual amplitude and annual phase (Table 2). The difference of annual phase between Radiosonde, GPS and MODIS-PWV is about  $1^\circ$ – $2^\circ$  at all stations, while there are a little differences in semi-annual phases at IZMI and ISPT stations. The annual amplitudes at most of the stations are similar, and large annual amplitudes are found at ADAN and SAMN stations, which are located at the coast of the Mediterranean Sea and the Black Sea, respectively.

##### 4.2. Long-term PWV trend

The PWV trends are further investigated. The trends of GPS-estimated PWV and Radiosonde PWV agree well (Table 2). At the GPS stations that are close to the coastline, GPS-estimated PWV trend agrees with Radiosonde, such as SAMN and ISTN stations with differences of  $0.01$ – $0.03 \text{ mm year}^{-1}$  respectively. However, at inland stations differences between GPS-estimated PWV and Radiosonde PWV trends reach  $0.2 \text{ mm year}^{-1}$ , which is still a good agreement.

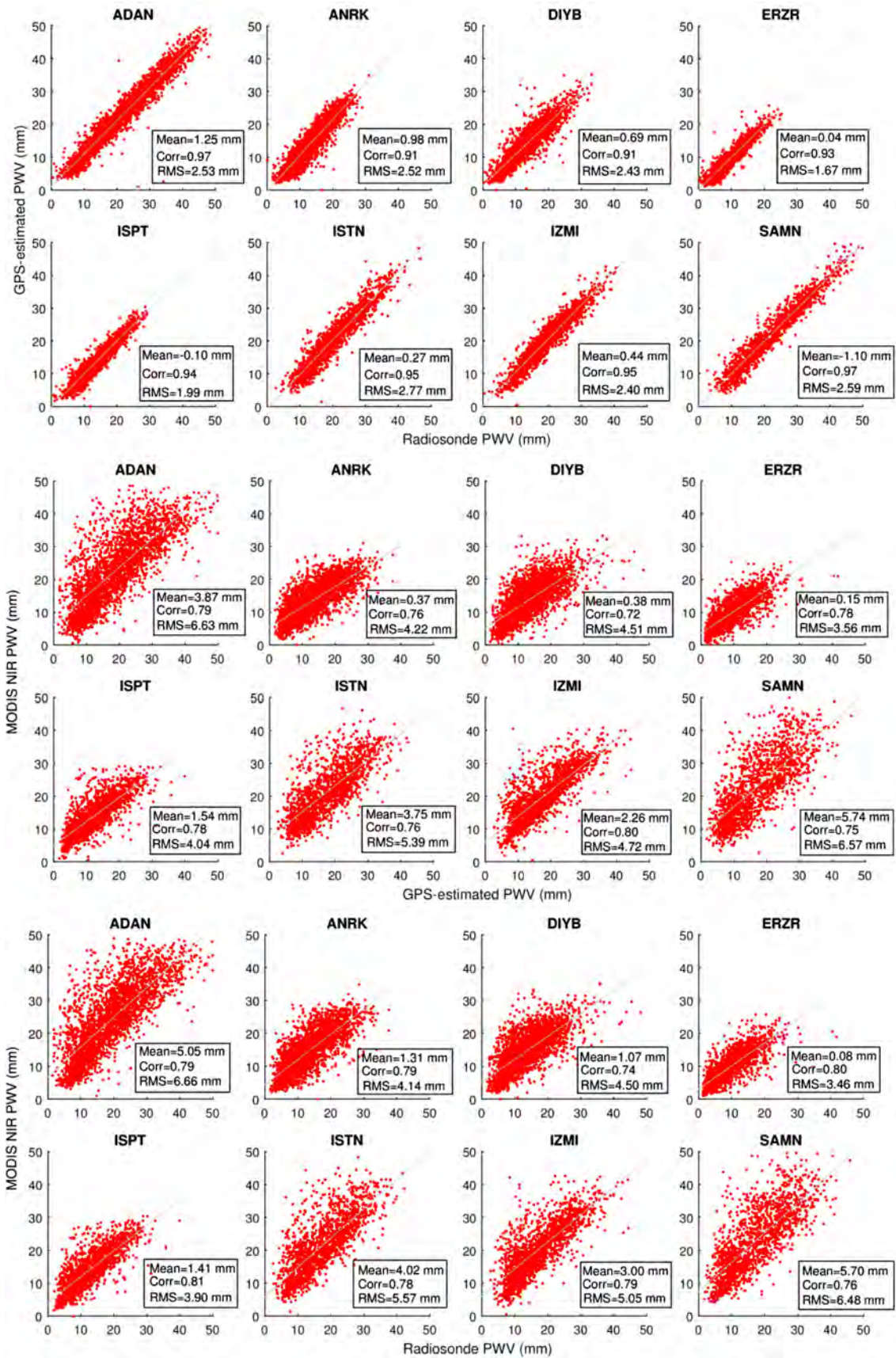


Figure 3. Correlations of PWV between MODIS, GPS and Radiosonde for all the locations. [Colour figure can be viewed at wileyonlinelibrary.com].

Table 1. Mean differences, correlation and RMSE values of PWV between GPS, Radiosonde and MODIS.

Measurements		ADAN	ANRK	DIYB	ERZR	ISPT	ISTN	IZMI	SAMN
GPS–Radiosonde	Mean (mm)	1.25	0.98	0.69	0.04	−0.1	0.27	0.44	−1.1
	Correlation	0.97	0.91	0.91	0.93	0.94	0.95	0.95	0.97
	RMSE (mm)	2.53	2.52	2.43	1.67	1.99	2.77	2.4	2.59
MODIS–GPS	Mean (mm)	3.87	0.37	0.38	0.15	1.54	3.75	2.26	5.74
	Correlation	0.79	0.76	0.72	0.78	0.78	0.76	0.8	0.75
	RMSE (mm)	6.63	4.22	4.51	3.56	4.04	5.39	4.72	6.57
MODIS–Radiosonde	Mean (mm)	5.05	1.31	1.07	0.08	1.41	4.02	3	5.7
	Correlation	0.79	0.79	0.74	0.8	0.81	0.78	0.79	0.76
	RMSE (mm)	6.66	4.14	4.5	3.46	3.9	5.57	5.05	6.48

Table 2. Trend, annual and semi-annual amplitude, and phase values obtained from different techniques at co-located GPS and radiosonde stations.

Stations	Type	Trend (mm year <sup>−1</sup> )	Annual phase (°)	Semi-annual phase (°)	Annual amplitude (mm)	Semi-annual amplitude (mm)
ADAN	GPS	0.30 ± 0.07	69.72 ± 0.02	29.99 ± 0.08	11.80 ± 0.17	2.17 ± 0.17
	MODIS	−0.27 ± 0.07	63.82 ± 0.02	27.83 ± 0.07	10.08 ± 0.17	2.35 ± 0.17
ANRK	Radiosonde	0.18 ± 0.07	68.38 ± 0.02	20.92 ± 0.08	12.32 ± 0.18	2.22 ± 0.17
	GPS	0.11 ± 0.04	70.29 ± 0.03	79.96 ± 0.11	4.92 ± 0.11	1.01 ± 0.11
DIYB	MODIS	−0.01 ± 0.05	68.39 ± 0.03	54.55 ± 0.09	6.14 ± 0.13	1.47 ± 0.13
	Radiosonde	0.19 ± 0.05	68.89 ± 0.02	60.27 ± 0.10	6.41 ± 0.12	1.16 ± 0.12
ERZR	GPS	0.12 ± 0.05	70.88 ± 0.04	52.84 ± 0.11	4.56 ± 0.13	1.14 ± 0.13
	MODIS	−0.12 ± 0.05	66.16 ± 0.03	−33.07 ± 1.88	5.86 ± 0.14	0.07 ± 0.13
ISPT	Radiosonde	−0.03 ± 0.05	69.29 ± 0.03	52.93 ± 0.12	5.09 ± 0.14	1.03 ± 0.13
	GPS	0.11 ± 0.05	70.34 ± 0.03	53.22 ± 0.23	4.86 ± 0.12	0.50 ± 0.12
ISTN	MODIS	−0.02 ± 0.06	73.24 ± 0.03	75.82 ± 0.49	5.62 ± 0.15	0.29 ± 0.14
	Radiosonde	0.06 ± 0.04	70.12 ± 0.03	28.70 ± 0.17	5.52 ± 0.11	0.64 ± 0.11
IZMI	GPS	0.30 ± 0.06	66.57 ± 0.04	76.29 ± 0.17	5.53 ± 0.16	0.89 ± 0.15
	MODIS	0.01 ± 0.07	68.39 ± 0.04	59.23 ± 0.15	5.93 ± 0.17	1.13 ± 0.16
SAMN	Radiosonde	0.16 ± 0.06	67.75 ± 0.03	60.87 ± 0.14	6.17 ± 0.15	1.12 ± 0.15
	GPS	0.32 ± 0.08	60.89 ± 0.03	60.70 ± 0.14	8.18 ± 0.19	1.39 ± 0.19
ANRK	MODIS	0.01 ± 0.07	62.57 ± 0.03	39.02 ± 0.10	8.37 ± 0.17	1.72 ± 0.17
	Radiosonde	0.29 ± 0.08	61.87 ± 0.03	58.71 ± 0.12	8.91 ± 0.21	1.69 ± 0.21
DIYB	GPS	0.35 ± 0.08	59.98 ± 0.03	−69.16 ± 0.24	6.76 ± 0.19	0.78 ± 0.19
	MODIS	0.01 ± 0.07	62.98 ± 0.03	47.60 ± 0.14	8.01 ± 0.17	1.16 ± 0.17
ERZR	Radiosonde	0.24 ± 0.08	61.88 ± 0.03	89.73 ± 0.22	7.45 ± 0.20	0.90 ± 0.20
	GPS	0.14 ± 0.08	64.13 ± 0.02	41.65 ± 0.11	11.12 ± 0.20	1.86 ± 0.20
ISTN	MODIS	−0.06 ± 0.08	65.70 ± 0.03	27.02 ± 0.10	9.10 ± 0.19	1.95 ± 0.19
	Radiosonde	0.15 ± 0.08	65.05 ± 0.02	42.52 ± 0.11	11.36 ± 0.21	1.89 ± 0.21

About MODIS NIR PWV and Radiosonde PWV trends relation, as it can be clearly seen in Table 2, MODIS NIR PWV trend agrees well with Radiosonde but not well as GPS-estimated PWV trend. Especially at the stations near coastal areas, the difference between trends reaches 0.5 mm year<sup>−1</sup> like at ADAN station. At IZMI and ISTN stations differences between MODIS NIR PWV and Radiosonde PWV trends are 0.3 and 0.25 mm year<sup>−1</sup>. However, at inland stations like DIYB or ERZR, trends agree well under 0.1 mm year<sup>−1</sup>. As stated in Section 3, MODIS tends to overestimate at locations with high PWV values near coastal areas which have humid weather with high temperatures. GPS-estimated PWV and MODIS NIR PWV trends have the highest differences in this inter-comparison. Same as MODIS NIR PWV and GPS-estimated PWV trends, stations at coastal areas have highest differences with 0.57 mm year<sup>−1</sup> as at ADAN station, while stations at inland with drier climate and low

temperature have less trend difference of 0.12 mm year<sup>−1</sup>, such as ANRK station.

The Kendall's Tau trend test results are further obtained. Kendall's Tau measures the extent of monotonic dependence that is a more robust measurement, being also resistant against the effect of outliers and the *P*-value that provides information about the significance of the trend. The smaller the *P*-value is, the more likely the trend is, e.g. the more likely the rejection of the null hypothesis. As an example, it is desired that the trend is captured at a confidence level of 95% (significance level of 0.05), and the *P*-value needs to be smaller than 0.05 while Kendall's Tau value gives the direction of the trend (increasing or decreasing). In Table 3, column 3 for Mann–Kendall and column 6 for seasonal Mann–Kendall, significant *P*-values are found at all the stations with the confidence level of 95% ranging from 0.0001 to 0.0161. These results indicate that all stations exhibit significant trends (increasing).

Table 3. Results of the Mann–Kendall and the seasonal Mann–Kendall trend tests.

Stations	Mann–Kendall trend test			Seasonal Mann–Kendall test			$\alpha$
	Kendall's Tau	P-value	Sen's slope	Kendall's Tau	P-value	Sen's slope	
ADAN	0.0479	<0.0001	0.0010	0.0508	0.0001	0.0723	0.05
ANKR	0.0334	0.0078	0.0004	0.0317	0.0161	0.0244	0.05
DIYB	0.0363	0.0030	0.0004	0.0415	0.0012	0.0262	0.05
ERZR	0.0553	0.0007	0.0008	0.0797	<0.0001	0.0669	0.05
ISPT	0.0722	<0.0001	0.0014	0.0847	<0.0001	0.1434	0.05
ISTN	0.0684	<0.0001	0.0019	0.0901	<0.0001	0.1680	0.05
IZMI	0.0762	<0.0001	0.0018	0.0902	<0.0001	0.1352	0.05
SAMN	0.0314	0.0041	0.0011	0.0608	0.0011	0.1425	0.05

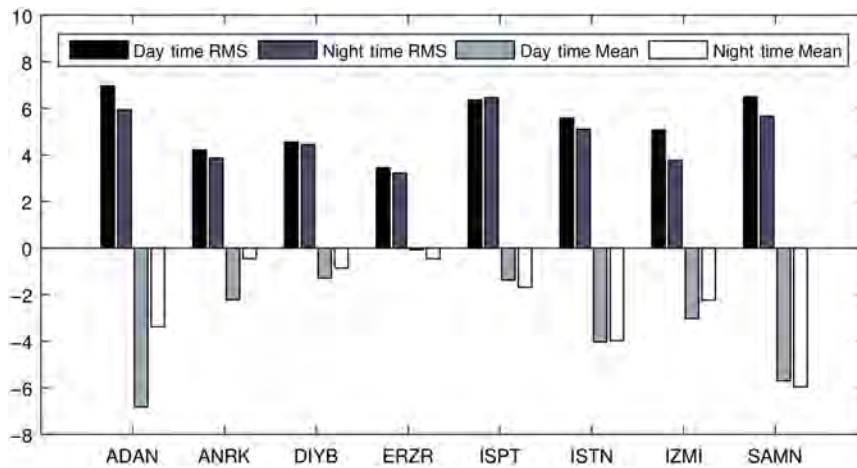


Figure 4. RMSE of MODIS IR PWV mean differences between the day time and night time. [Colour figure can be viewed at wileyonlinelibrary.com].

4.3. Effects and discussions

Figure 6 show PWV trends at co-located GPS and Radiosonde stations. It can be seen that the higher PWV trends are found at the west and south part of Turkey, which are near the Aegean Sea and the Mediterranean Sea coasts with a connection to the Atlantic Ocean. This also could be an indication to the effect of climate oscillations like NAO or ENSO.

The NAO occurs because of the fluctuations of atmospheric pressure differences between two pressure centres at sea level of northern part of the Atlantic Ocean. As stated

in climatology studies related to oscillation indexes, one of the central pressure points with the low-pressure point is located near Iceland and the second one is over Azores island chain in the eastern part of the Atlantic Ocean. The fluctuations occurring between low- and high-pressure centres controls the degree of strength of winds and storm tracks in the north Atlantic. The daily NAO index corresponds to the NAO patterns, which varies from month to month. Rotated Principal Component Analysis (RPCA) was used to calculate the daily PNA and NAO teleconnection indices (Barnston and Livezey, 1987). The monthly

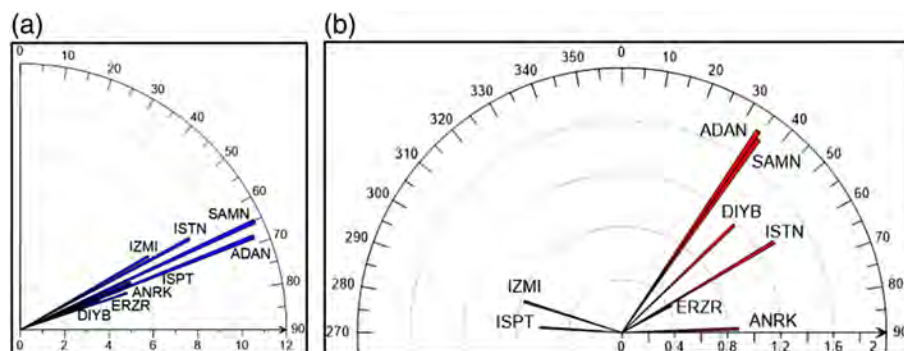


Figure 5. (a) Annual phase ( $^{\circ}$ ) and amplitude (mm) of GPS-estimated PWV. (b) Semi-annual phase ( $^{\circ}$ ) and amplitude (mm) of GPS-estimated PWV. [Colour figure can be viewed at wileyonlinelibrary.com].

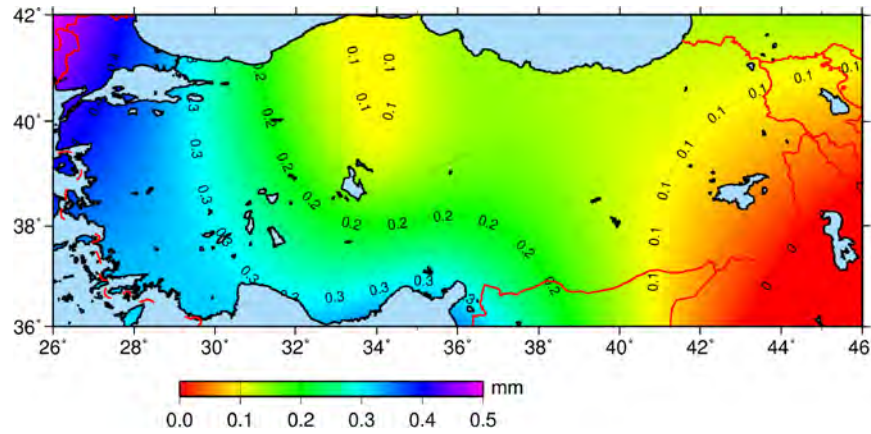


Figure 6. Distribution of GPS-estimated PWV trends. [Colour figure can be viewed at wileyonlinelibrary.com].

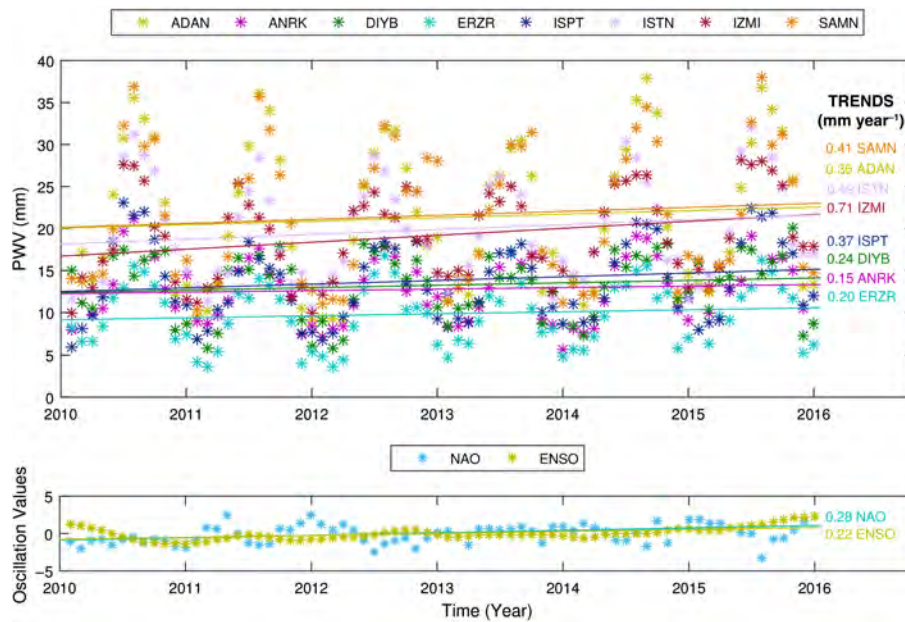


Figure 7. Comparison of PWV and oscillation trends from monthly mean values. [Colour figure can be viewed at wileyonlinelibrary.com].

teleconnection patterns are linearly interpolated to the day if needed and therefore account for the seasonality inherent in the NAO patterns. The NAO has two phases, positive phase and negative phase. Continuous measurements around the Atlantic Ocean designate the index values of the NAO which indicates the phases of NAO (Hurrell, 1995). In the positive NAO phase which is the case in this study, pressure changes between two centres result in a decrease in storm counts and low precipitation (NOAA, 2009). As an example, the Maltese Islands in the Mediterranean Sea registered as one of the driest years ever recorded up to the beginning of March 2015 as the Island’s national average was only 235 mm while some areas was even less than 200 mm in 2015.

In this study, monthly NAO and ENSO index values are used. The relationship between GPS-PWV trend and oscillation indexes is obtained (Figure 7). The trends of GPS-estimated PWV are different from the trends represented in Table 2. The overall trend of NAO is

positive through evaluated PWV period in this study. As the definition of positive NAO phase, pressure is increased, and precipitation is dropped in most parts of the Turkey, like ADAN station which is near the coastline of Mediterranean Sea (Figure 8). The western and southern parts of the Turkey show similar patterns to the Maltese Islands in the Mediterranean Sea. While pressure is increasing, the precipitation and humidity are decreasing at ADAN station. This variation fits well with the positive NAO phase.

Although meteorological parameters are consistent with NAO indexes, PWV computed in this study does not match with the precipitation and humidity data. For NAO phase to be positive, temperature and pressure should increase while precipitation decreases like drought. This temperature increase also can be proven by computation of land surface temperatures (Sekertekin *et al.*, 2016). However, PWV trends found in this study are increasing, which do not agree with meteorological data. This difference may

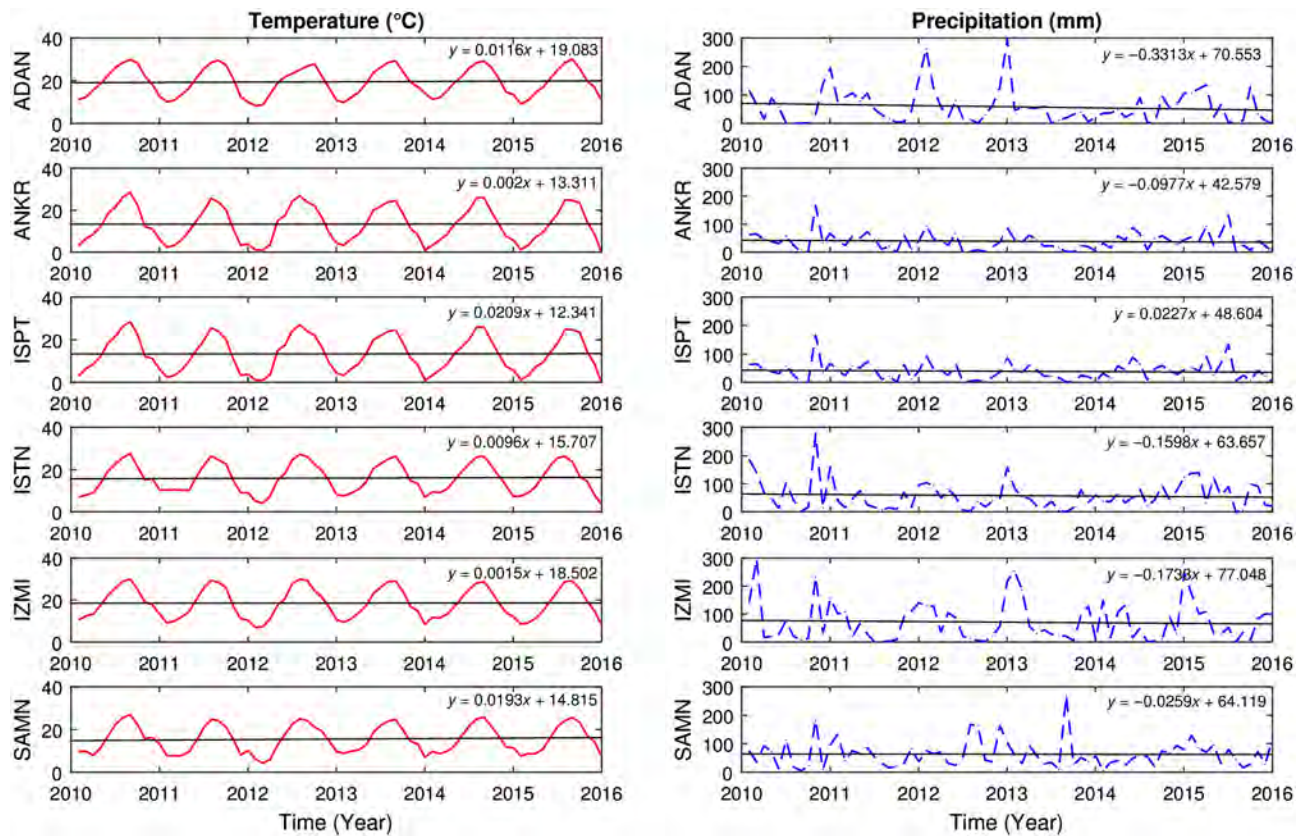


Figure 8. Variations of temperature and precipitation from 2010 to 2016. [Colour figure can be viewed at [wileyonlinelibrary.com](http://wileyonlinelibrary.com)].

result from human activities impact recently (e.g. societal, coal plants, construction) (Roman *et al.*, 2015). Also, population growth and construction of new coal plants that release an immense amount of water vapour to the troposphere may also affect PWV variation trend.

## 5. Conclusions

In this study, the long-term trend behaviours and spatiotemporal variations of PWV over Turkey are investigated. Firstly, PWV time series are estimated and evaluated from GPS, MODIS and Radiosonde. Secondly, different  $T_m$  models, mapping functions and OTL models are evaluated, which shows that the best GPS results are obtained with Bevis  $T_m$  model, VMF1 and FES2004 OTL. Also, different retrieval strategies, day and night differences are investigated for MODIS-PWV values. Accuracies of MODIS-PWV both IR and NIR were tested for the first time in Turkey using an extended period data.

Furthermore, the long-term trend and seasonal variations of PWV time series from three techniques are analyzed. It has shown that the PWV values have a strong seasonal signal, which agrees well for nearly all strategies used in this study. The annual phases of Radiosonde, GPS, and MODIS-PWVs at all the stations are almost close to each other. Statistically significant increasing trends are found at all stations.

Finally, the relations between PWV trends, and oscillation indexes are obtained. Since the NAO is more related to the Mediterranean Sea than the ENSO, the NAO behaviours with meteorological parameters are investigated. The overall trend of the NAO is positive through evaluated PWV period in this study, and observed meteorological parameters agrees with positive NAO phase. However, PWV trends do not agree with meteorological data, which may be due to the effects of recent human activities.

## Acknowledgements

The study was partially performed at TUBITAK ULAK-BIM, High Performance and Grid Computing Center (TRUBA resources). The authors are grateful to the organizations that provided the data, including General Command of Mapping (HGK) for TUSAGA-Active data, Turkish Met-Office (MGM) for meteorological data, National Aeronautics and Space Administration (NASA), Atmosphere Archive and Distribution System (LAADS) for MODIS data and International GNSS Service (IGS) for daily RINEX and final products.

## References

- Afraimovich E, Ding F, Kiryushkin V, Yasyukevich Y, Jin SG. 2010. TEC response to the 2008 Wenchuan earthquake in comparison with

- other strong earthquakes. *Int. J. Remote Sens.* **31**(13): 3601–3613. <https://doi.org/10.1080/01431161003727747>.
- Albek E. 2002. Statistical analysis of water quality trends: an application to the Porsuk Stream. *Anadolu Univ. J. Sci. Technol.* **3**(2): 281–292.
- Asrar G, Greenstone R. 1995. *MTPE EOS Reference Handbook*. NASA Goddard Space Flight Center Tech. Rep., Washington DC, 277 pp.
- Barnston AG, Livezey RE. 1987. Classification, seasonality and persistence of low-frequency atmospheric circulation patterns. *Mon. Weather Rev.* **115**: 1083–1126.
- Bevis M, Businger S, Herring TA, Rocken C, Anthes R, Ware R. 1992. GPS meteorology: remote sensing of atmospheric water vapour using the global positioning system. *J. Geophys. Res.* **97**: 15787–15801. <https://doi.org/10.1029/92JD01517>.
- Bevis M, Chiswell S, Hering TA, Anthes R, Rocken C, Ware R. 1994. GPS meteorology: mapping Zenith wet delays onto precipitable water. *J. Appl. Meteorol.* **33**: 379–386. [https://doi.org/10.1175/1520-0450\(1994\)033<0379:GMMZWD>2.0.CO;2](https://doi.org/10.1175/1520-0450(1994)033<0379:GMMZWD>2.0.CO;2).
- Boehm J, Werl B, Schuh H. 2006. Troposphere mapping functions for GPS and very long baseline interferometry from European Center for Medium-Range Weather Forecasts operational analysis data. *J. Geophys. Res.* **111**: B02406. <https://doi.org/10.129/2005JB003629>.
- Chaboureaud JP, Che´din A, Scott NA. 1998. Remote sensing of the vertical distribution of the atmospheric water vapour from the TOVS observations: method and validation. *J. Geophys. Res.* **103**: 8743–8752. <https://doi.org/10.1029/98JD00045>.
- Chang L, Jin SG, He X. 2014. Assessment of InSAR atmospheric correction using both MODIS Near-Infrared and Infrared water vapour products. *IEEE Trans. Geosci. Remote Sens.* **52**(9): 5726–5735.
- Eanes RJ. 1994. Diurnal and semidiurnal tides from TOPEX/POSEIDON altimetry. *Eos. Trans. AGU* **75**(16): 108. <https://doi.org/10.1029/2003GL017676>.
- Ferrare R, Brasseur L, Clayton M, Turner D, Remer L, Gao BC. 2002. Evaluation of TERRA aerosol and water vapour measurements using ARM SGP data. In *Paper Presented at the American Meteorological Society 11th Conference on Atmospheric Radiation*, Ogden, Utah, 3–7 June 2002.
- Gao BC, Kaufman YJ. 2003. Water vapour retrievals using moderate resolution imaging spectroradiometer (MODIS) near-infrared channels. *J. Geophys. Res.* **108**(D13): 4389. <https://doi.org/10.1029/2002JD003023>.
- Gilbert RO. 1987. *Statistical Methods for Environmental Pollution Monitoring*. Wiley: New York.
- Gurbuz G, Jin SG. 2016. Evaluation of ocean tide loading effects on GPS-estimated precipitable water vapour in Turkey. *Geod. Geodyn.* **7**: 32–38. <https://doi.org/10.1016/j.geog.2015.12.008>.
- Held IM, Soden BJ. 2000. Water vapour feedback and global warming. *Ann. Rev. Energy Environ.* **25**: 441–475. <https://doi.org/10.1146/annurev.energy.25.1.441>.
- Herring T, King R, Floyd M, McClusky S. 2015. *Introduction to GAMIT/GLOBK*. Massachusetts Institute of Technology: Cambridge, MA.
- Hirsch RM, Slack JR, Smith RA. 1982. Techniques of trend analysis for monthly water quality data. *Water Resour. Res.* **18**(1): 107–121.
- Hurrell JW. 1995. Decadal trends in the North Atlantic Oscillation regional temperatures and precipitation. *Science* **269**: 676–679. <https://doi.org/10.1126/science.269.5224.676>.
- Jin SG, Wang J, Zhang H, Zhu W. 2004. Real-time monitoring and prediction of the total ionospheric electron content by means of GPS observations. *Chin. Astron. Astrophys.* **28**(3): 331–337. <https://doi.org/10.1016/j.chinastron.2004.07.008>.
- Jin SG, Park P. 2006. Strain accumulation in South Korea inferred from GPS measurements. *Earth Planets Space* **58**(5): 529–534. <https://doi.org/10.1186/BF03351950>.
- Jin SG, Park J, Wang J, Choi B, Park P. 2006. Electron density profiles derived from ground-based GPS observations. *J. Navig.* **59**(3): 395–401.
- Jin SG, Cho J, Park J. 2007a. Ionospheric slab thickness and its seasonal variations observed by GPS. *J. Atmos. Sol.-Terr. Phys.* **69**(15): 1864–1870. <https://doi.org/10.1016/j.jastp.2007.07.008>.
- Jin SG, Park J, Cho J, Park P. 2007b. Seasonal variability of GPS-derived Zenith tropospheric delay (1994–2006) and climate implications. *J. Geophys. Res.* **112**: D09110. <https://doi.org/10.1029/2006JD007772>.
- Jin SG, Li ZC, Cho JH. 2008. Integrated water vapour field and multi-scale variations over China from GPS measurements. *J. Appl. Meteorol. Clim.* **47**: 3008–3015. <https://doi.org/10.1175/2008JAMC1920.1>.
- Jin SG, Luo OF. 2009. Variability and climatology of PWV from global 13-year GPS observations. *IEEE Trans. Geosci. Remote Sens.* **47**: 1918–1924. <https://doi.org/10.1109/TGRS.2008.2010401>.
- Jin SG, Luo OF, Gleason S. 2009. Characterization of diurnal cycles in ZTD from a decade of global GPS observations. *J. Geophys. Res.* **83**: 537–545. <https://doi.org/10.1007/s00190-008-0264-3>.
- Jin SG, Feng GP, Gleason S. 2011a. Remote sensing using GNSS signals: current status and future directions. *Adv. Space Res.* **47**: 1645–1653. <https://doi.org/10.1016/j.asr.2011.01.036>.
- Jin SG, Han L, Cho J. 2011b. Lower atmospheric anomalies following the 2008 Wenchuan earthquake observed by GPS measurements. *J. Atmos. Sol.-Terr. Phys.* **73**(7–8): 810–814. <https://doi.org/10.1016/j.jastp.2011.01.023>.
- Jin SG, Feng GP. 2013. Large-scale variations of global groundwater from satellite gravimetry and hydrological models, 2002–2012. *Global Planet. Change* **106**: 20–30. <https://doi.org/10.1016/j.gloplacha.2013.02.008>.
- Jin SG, Jin R, Li J. 2014a. Pattern and evolution of seismo-ionospheric disturbances following the 2011 Tohoku earthquakes from GPS observations. *J. Geophys. Res.* **119**(9): 7914–7927. <https://doi.org/10.1002/2014JA019825>.
- Jin SG, Cardellach E, Xie F. 2014b. *GNSS Remote Sensing: Theory, Methods and Applications*. Springer: the Netherlands. ISBN: 978-94-007-7481-0, 276 pp.
- Jin SG, Occhipinti G, Jin R. 2015. GNSS ionospheric seismology: Recent observation evidences and characteristics. *Earth-Sci. Rev.* **147**: 54–64.
- Jin SG, Jin R, Li D. 2016. Assessment of BeiDou differential code bias variations from multi-GNSS network observations. *Ann. Geophys.* **34**(2): 259–269. <https://doi.org/10.5194/angeo-34-259-2016>.
- Jin SG, Jin R, Li D. 2017. GPS detection of ionospheric Rayleigh wave and its source following the 2012 Haida Gwaii earthquake. *J. Geophys. Res. Space Physics* **122**(1): 1360–1372.
- Kaufman YJ, Gao B. 1992. Remote sensing of water vapour in the near IR from EOS/MODIS. *IEEE Trans. Geosci. Remote Sens.* **30**: 871–884. <https://doi.org/10.1109/36.175321>.
- Kendall MG. 1975. *Rank Correlation Methods*, 4th edn. Charles Griffin: London.
- King MD, Kaufman YJ, Menzel WP, Tanre D. 1992. Remote-sensing of cloud, aerosol, and water vapour properties from the moderate resolution imaging spectrometer (MODIS). *IEEE Trans. Geosci. Remote Sens.* **30**: 2–27. <https://doi.org/10.1109/36.124212>.
- King MD, Menzel WP, Kaufman YJ, Tanre D, Gao BC, Platnick S, Ackerman SA, Remer LA, Pincus R, Hubanks PA. 2003. Cloud and aerosol properties, precipitable water, and profiles of temperature and water vapour from MODIS. *IEEE Trans. Geosci. Remote Sens.* **41**: 442–458. <https://doi.org/10.1109/TGRS.2002.808226>.
- Liu H, Tang S, Zhang S, Hu J. 2015. Evaluation of MODIS water vapour products over China using radiosonde data. *Int. J. Remote Sens.* **36**: 680–690. <https://doi.org/10.1080/01431161.2014.999884>.
- Lyard F, Lefevre F, Letellier T, Francis O. 2006. Modelling the global ocean tides: modern insights from FES2004. *Ocean Dyn.* **56**(5): 394–415. <https://doi.org/10.1007/s10236-006-0086>.
- Mann HB. 1945. Nonparametric tests against trend. *Econometrica* **13**(3): 245–259.
- Matsumoto K, Takanezawa T, Ooe M. 2000. Ocean tide models developed by assimilating TOPEX/POSEIDON altimeter data into hydrodynamical model: a global model and a regional model around Japan. *J. Oceanogr.* **56**: 567–581. <https://doi.org/10.1023/A:1011157212596>.
- Mockler SB. 1995. Water Vapor in the Climate System, Special Report AGU, Washington, DC.
- Niell AB. 1996. Global mapping functions for the atmosphere delay at radio wavelengths. *J. Geophys. Res.* **101**: 3227–3246. <https://doi.org/10.1029/95JB03048>.
- NOAA. 2009. North Atlantic Oscillation of National Oceanic and Atmospheric Administration (NOAA) Climate Prediction Center (accessed 27 August 2016).
- Ray RD. 1999. A global ocean tide model from TOPEX/POSEIDON altimetry: GOT99.2. *NASA Tech. Memo.* 209478, 58. Report ID: NASA/TM-1999-209478.
- Roman J, Knuteson R, Ackerman S, Revercomb H. 2015. Predicted changes in the frequency of extreme precipitable water vapour events. *J. Clim.* **28**: 7057–7070.
- Salomonson VV, Barnes WL, Maymon PW, Montgomery HE, Ostrow H. 1989. MODIS: advanced facility instrument for studies of the earth as a system. *IEEE Trans. Geosci. Remote Sens.* **27**(2): 145–153.
- Seemann SW, Li J, Menzel WP, Gumley LE. 2003. Operational retrieval of atmospheric temperature, moisture, and ozone from MODIS infrared radiances. *J. Appl. Meteorol.* **42**: 1072–1091. [https://doi.org/10.1175/1520-0450\(2003\)042<1072:OROATM>2.0.CO;2](https://doi.org/10.1175/1520-0450(2003)042<1072:OROATM>2.0.CO;2).

- Seemann SW, Borbas EE, Knuteson RO, Stephenson GR, Huang HL. 2008. Development of a global infrared land surface emissivity database for application to clear sky sounding retrievals from multi-spectral satellite radiance measurements. *J. Appl. Meteorol. Climatol.* **47**: 108–123. <https://doi.org/10.1175/2007jamc1590.1>.
- Sekertekin A, Kutoglu SH, Kaya S. 2016. Evaluation of spatio-temporal variability in land surface temperature: a case study of Zonguldak, Turkey. *Environ. Monit. Assess.* **188**(1): 30.
- Tregoning P, van Dam T. 2005. Atmospheric pressure loading corrections applied to GPS data at the observation level. *Geophys. Res. Lett.* **32**: L22310. <https://doi.org/10.1029/2005GL024104>.
- Trenberth KE, Fasullo J, Smith L. 2005. Trends and variability in column-integrated atmospheric water vapour. *Clim. Dyn.* **24**: 741–758. <https://doi.org/10.1007/s00382-005-0017-4>.
- Trenberth KE, John TF, Jeffrey K. 2009. Earth's global energy budget. *Bull. Am. Meteorol. Soc.* **90**(3): 311–323.
- Tuka A, El-Mowafy A. 2013. Performance evaluation of different troposphere delay models and mapping functions. *Measurement* **46**: 928–937. <https://doi.org/10.1016/j.measurement.2012.10.015>.
- Wagner T, Beirle S, Grzegorski M, Platt U. 2006. Global trends (1996–2003) of total column precipitable water observed by global ozone monitoring experiment (GOME) on ERS-2 and their relation to near-surface temperature. *J. Geophys. Res.* **111**: D12102. <https://doi.org/10.1029/2005jd006523>.
- Wang J, Zhang L, Dai A, Van Hove T, Van Baelen J. 2007. A near-global, 2-hourly data set of atmospheric precipitable water from ground-based GPS measurements. *J. Geophys. Res.* **112**: D11107. <https://doi.org/10.1029/2006JD007529>.
- Wang J, Cole HL, Carlson DJ, Miller ER, Beierle K. 2002. Corrections of humidity measurement errors from the Vaisala RS80 radiosonde: application to TOGA COARE data. *J. Atmos. Oceanic Tech.* **19**: 981–1002. [https://doi.org/10.1175/1520-0426\(2002\)019<0981:COHMEF>2.0.CO;2](https://doi.org/10.1175/1520-0426(2002)019<0981:COHMEF>2.0.CO;2).
- Ware RH, Fulker DW, Stein SA, Anderson DN, Avery SK, Clark RD, Droegemeier KK, Kuettner JP, Minster JB, Sorooshian S. 2000. Suominet: a real-time national GPS network for atmospheric research and education. *Bull. Am. Meteorol. Soc.* **81**: 677–694. [https://doi.org/10.1175/1520-0477\(2000\)081<0677:SARNGN>2.3.CO;2](https://doi.org/10.1175/1520-0477(2000)081<0677:SARNGN>2.3.CO;2).
- Wu Y, Jin SG, Wang Z, Liu J. 2010. Cycle slip detection using multi-frequency GPS carrier phase observations: a simulation study. *Adv. Space Res.* **46**(2): 144–149. <https://doi.org/10.1016/j.asr.2009.11.007>.